Acta Crystallographica Section D
Biological Crystallography
ISSN 0907-4449

Analysis of three crystal structure determinations of a 5-methyl-6-*N*-methylanilino pyridopyrimidine antifolate complex with human dihydrofolate reductase

Vivian Cody,[a]* Joseph R. Luft,[a] Walter Pangborn[a] and Aleem Gangjee[b]

[a]Structural Biology Department, Hauptman–Woodward Medical Research Institute Inc., 73 High Street, Buffalo, NY 14203, USA, and [b]Division of Medicinal Chemistry, Graduate School of Pharmaceutical Sciences, Duquesne University, Pittsburgh, PA 15282, USA

Correspondence e-mail: cody@hwi.buffalo.edu

Received 19 May 2003
Accepted 8 July 2003

PDB References: *R*3-1, 1pd8, r1pd8; *R*3-2, 1pd9, r1pd9; $P4_32_12$ lattice, 1pdb, r1pdb.

Structural data are reported for the first example of the potent antifolate inhibitor 2,4-diamino-5-methyl-6-[(3′,4′,5′-trimethoxy-*N*-methylanilino)methyl]pyrido[2,3-*d*]pyrimidine (1) in complex with human dihydrofolate reductase (hDHFR) and NADPH. Small differences in crystallization conditions resulted in the growth of two different forms of a binary complex. The structure determination of an additional crystal of a ternary complex of hDHFR with NADPH and (1) grown under similar conditions is also reported. Diffraction data were collected to 2.1 Å resolution for an *R*3 lattice from a hDHFR ternary complex with NADPH and (1) and to 2.2 Å resolution from a binary complex. Data were also collected to 2.1 Å resolution from a binary complex with hDHFR and (1) in the first example of a tetragonal $P4_32_12$ lattice. Comparison of the intermolecular contacts among these structures reveals differences in the backbone conformation (1.9–3.2 Å) for flexible loop regions (residues 40–46, 77–83 and 103–107) that reflect differences in the packing environment between the rhombohedral and tetragonal space groups. Analysis of the packing environments shows that the tetragonal lattice is more tightly packed, as reflected in its smaller V_M value and lower solvent content. The conformation of the inhibitor (1) is similar in all structures and is also similar to that observed for TMQ, the parent quinazoline compound. The activity profile for this series of 5-deaza *N*-substituted non-classical trimethoxybenzyl antifolates shows that the N10—CH_3 substituted (1) has the greatest potency and selectivity for *Toxoplasma gondii* DHFR (*tg*DHFR) compared with its N—H or N—CHO analogs. Models of the *tg*DHFR active site indicate preferential contacts with (1) that are not present in either the human or *Pneumocystis carinii* DHFR structures. Differences in the acidic residue (Glu30 *versus* Asp for *tg*DHFR) affect the precise positioning of the diaminopyrido-pyrimidine ring, while changes in other residues, particularly at positions 60 and 64 (Leu *versus* Met and Asn *versus* Phe), involve interactions with the trimethoxybenzyl substituents.

1. Introduction

Antifolates have been shown to be effective agents against dihydrofolate reductase (DHFR) from such pathogens as *Pneumocystis carinii* (*pc*) and *Toxoplasma gondii* (*tg*), which are major medical threats, particularly in those patients with immune-compromised conditions such as AIDS (Mills & Masur, 1991). Presently, treatment of these pathogens with trimethoprim (TMP) and trimetrexate (TMQ; Fig. 1) have limited success, as they are weak (TMP) or non-selective (TMQ) inhibitors of *pc*DHFR and *tg*DHFR (Masur *et al.*, 1993). Therefore, it is of interest to design antifolates with enhanced selectivity against these opportunistic pathogens

(Gangjee *et al.*, 1993, 1996, 1998; Queener, 1995; Piper *et al.*, 1996). To this end, a series of 2,4-diamino-5-methyl-6-(anilinomethyl)pyrido[2,3-*d*]pyrimidine antifolates were synthesized, which revealed a pattern of differential inhibitory potencies for N10-substituted analogs with variable methoxybenzyl substitutions (Gangjee *et al.*, 1993). These 5-deaza nonclassical antifolates with trimethoxy-, dichloro- or trichloro-substituted benzyl rings and with an N—H, N—CH_3 or N—CHO at position 10 were potent and selective inhibitors against *pc*DHFR, *tg*DHFR and rat liver DHFR (rlDHFR). Of these antifolates, the trimethoxybenzyl N10—CH_3 analog (1) (Fig. 1) was the most potent and selective (Table 1) (Gangjee *et al.*, 1993). For example, compound (1) was three times more potent and 17 times more selective for *tg*DHFR than TMQ and has greater selectivity for *tg*DHFR than its N10—H or N10—CHO analogs (Table 1). This pattern suggested that N10 substitution could be important for selectivity against *tg*DHFR and implied that steric and/or electronic restrictions of side-chain flexibility could play a role in these observations.

Although many assays of antifolate inhibitors of DHFR have been performed using rlDHFR as a target, the sequence of rlDHFR was not known until recently (Wang *et al.*, 2001). These data revealed that the rlDHFR sequence is 89% homologous to human DHFR (hDHFR) and that 33 of the 35 active-site residues are identical in the two sequences. However, to date structural details have not been reported for the rlDHFR enzyme. These sequence-alignment data indicate that the structural details of hDHFR can be used as a model to understand the correlation between structure and biological activity.

Sequence alignment of hDHFR, rlDHFR, *pc*DHFR and *tg*DHFR indicates that there are several conserved residues among these enzymes and that the active-site regions are highly homologous (Roos, 1993; Wang *et al.*, 2001). The most significant differences among these enzymes involve active-site residues 21, 30, 31, 35, 60 and 64 (human numbering) (Table 2). One of the more significant changes involves position 21 (Asp, Ser and Gly in hDHFR, *pc*DHFR and *tg*DHFR, respectively). In addition, changes at position 35 (Gln, Lys, Ser) are involved in contacts to the conserved Arg70. Structural data reveal that there is subdomain movement of the loop near residue 35, which moves towards the conserved Arg70 on binding non-classical inhibitors that do not possess a *p*-aminobenzylglutamate moiety (Gangjee *et al.*, 1998; Cody *et al.*, 1999). The strength of the hydrogen-bonding interactions between residue 35 and the conserved Arg70 would be affected by residue changes among these DHFR enzymes, which could also affect the selectivity of enzyme inhibition. Another important sequence change is position 60 (Leu, Leu and Met in hDHFR, *pc*DHFR and *tg*DHFR, respectively), which forms part of the hydrophobic pocket around the trimethoxylbenzyl ring of these inhibitors.

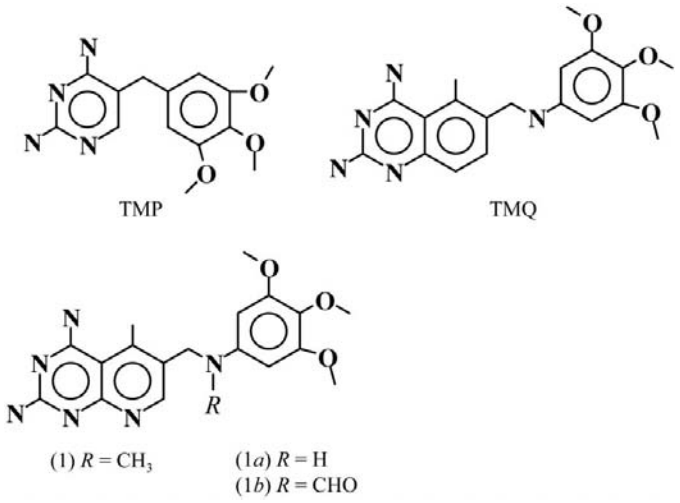

Figure 1
Schematic representation of trimethoprim (TMP), trimetrexate (TMQ) and its pyridopyrimidine N10-substituted analogs.

Table 1
Biological activity data (IC_{50}) and selectivity ratios reported for the antifolates shown in Fig. 1 (Gangjee *et al.*, 1993).

	IC_{50} (n*M*)			Selectivity ratio	
Analogue	*pc*DHFR	rlDHFR	*tg*DHFR	rlDHFR/ *pc*DHFR	rlDHFR/ *tg*DHFR
(1) $R = CH_3$	13.2	7.6	0.58	0.58	8.94
(1*a*) $R = H$	86	2.1	7.4	0.02	0.28
(1*b*) $R = CHO$	550	110	13.0	0.20	8.46
TMQ	42	3	10	0.07	0.3
TMP	12000	133000	2700	11.1	49

Table 2
Sequence comparison among DHFRs.

Residue†	hDHFR	rlDHFR	*pc*DHFR	*tg*DHFR
21	Asp	Asp	Ser	Gly
30	Glu	Glu	Glu	Asp
31	Phe	Phe	Ile	Phe
35	Gln	Gln	Lys	Ser
60	Ile	Ile	Ile	Met
64	Asn	Asn	Phe	Phe

† Human numbering.

To understand the pattern of potency and selectivity reported for this class of antifolates, the first crystallographic results are reported for analog (1) (Fig. 1) observed in three complexes with hDHFR. These structural results are compared with similar antifolate complexes with hDHFR (Cody *et al.*, 1993, 2003) and with *pc*DHFR (Cody *et al.*, 2000, 2002).

2. Experimental

2.1. Crystallization and X-ray data collection

Human DHFR was isolated and purified by Blakley as described in Chunduru *et al.* (1994) and crystals were grown by the hanging-drop vapor-diffusion method. The protein was washed in a Centricon-10 three times with 50 m*M* phosphate buffer pH 6.8 in 100 m*M* KCl buffer and concentrated to 10.0 mg ml^{-1}. Samples of hDHFR were incubated with NADPH and (1) overnight in the cold. The protein was

concentrated to 10.0 mg ml^{-1}. Protein droplets contained variable amounts of ammonium sulfate in 0.1 *M* phosphate buffer pH 8.0. Crystals grew over a five-month period and showed the presence of two different morphologies. Data were collected from a rhombohedral crystal (R3-1) grown in 62% ammonium sulfate, space group *R*3, that diffracted to 2.1 Å resolution. Crystals from an adjacent well (61% ammonium sulfate) were tetragonal, space group $P4_32_12$, and also diffracted to 2.1 Å resolution. When the protein plate was to be discarded after standing for several years, a protein crystal (R3-2) was noted in a well that had dried out and had originally contained 63% ammonium sulfate. The droplet was washed with 75% ammonium sulfate and the protein crystal screened. Diffraction data showed it was rhombohedral, space group *R*3, and diffracted to 2.2 Å resolution. The unit-cell parameters for these complexes of hDHFR are listed in Table 3. Data were collected at room temperature on a Rigaku R-AXIS IIc area detector and the data were processed and scaled with *DENZO* and *SCALEPACK*, respectively (Otwinowski & Minor, 1997). All data were refined to their resolution limits (Table 3).

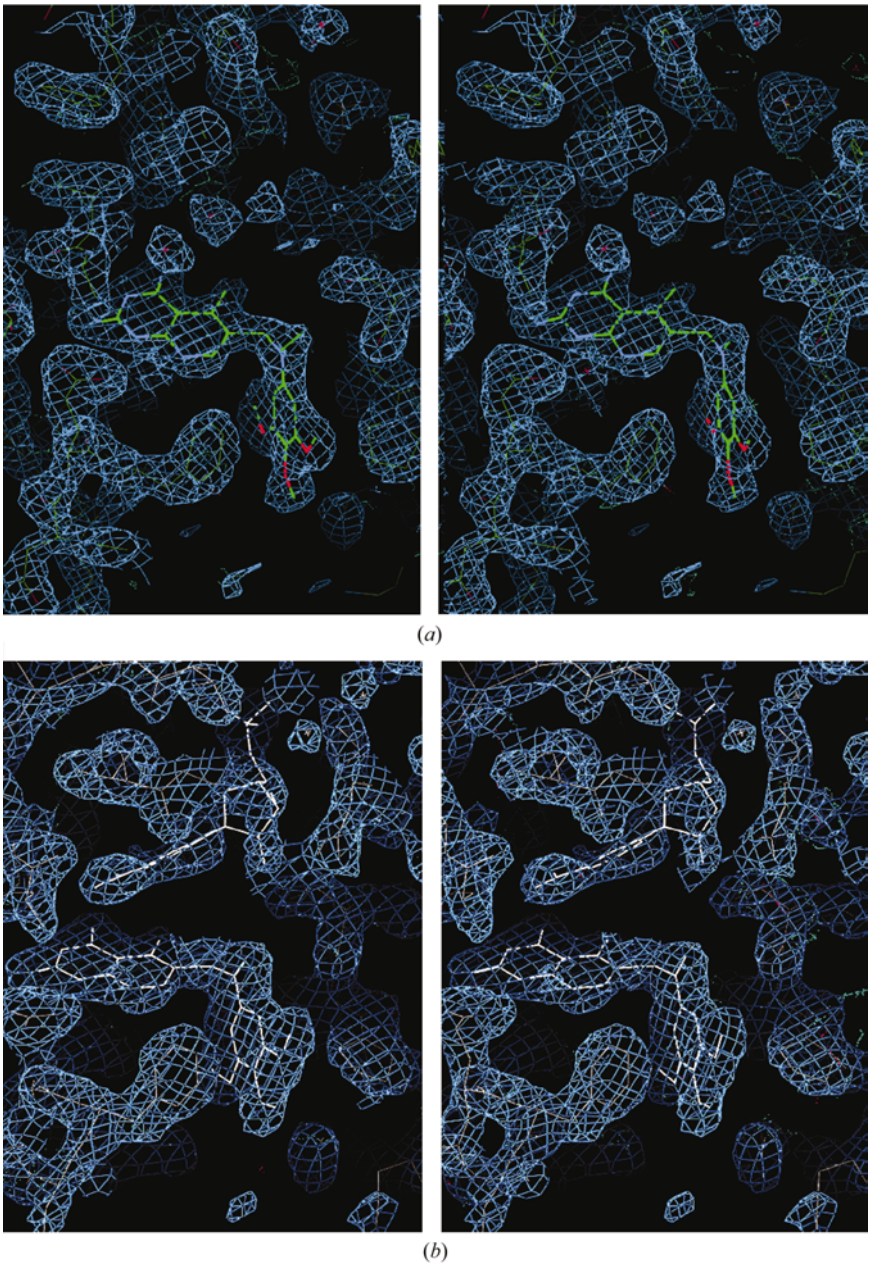

Figure 2
(*a*) Stereoview of $2F_o - F_c$ electron density (blue), using phases calculated from only the protein, in the *R*3 hDHFR–(1) binary complex, showing the fit of the enzyme and inhibitor (green) to the density. (*b*) Stereoview of $2F_o - F_c$ electron density (blue), using phases calculated from only the protein, in the *R*3 hDHFR–NADPH–(1) ternary complex, showing the fit of the enzyme, inhibitor and cofactor (white) to the density. The diagrams were produced with *CHAIN* (Sack, 1988).

2.2. Structure determination and refinement

The structures of these hDHFR–(1) complexes were solved by molecular-replacement methods using the restrained least-squares program *PROLSQ* (Hendrickson & Konnert, 1980; Finzel, 1987) in combination with the model-building program *CHAIN* (Sack, 1988). All calculations were carried out on a Silicon Graphics Impact R10000 Workstation. The initial $(2|F_o| - |F_c|)\exp(i\alpha_c)$ maps, where F_o are the observed and F_c are the calculated structure factors based on the protein model only and α_c is the calculated phase, resulted in electron density corresponding to the inhibitor but not the cofactor in two of the structures (Fig. 2). Refinement data showed that the structure of the rhombohedral crystal R3-1 (Table 3) was a ternary complex of NADPH and (1) with hDHFR, while the rhombohedral crystal R3-2 was a binary complex. Data for the first observation of a tetragonal crystal also revealed a binary complex. Two sulfate groups from the precipitating agent occupy the pyrophosphate positions of NADPH and water molecules fill the nicotinamide-ring pocket in the binary structures.

Further restrained refinement was continued for these complexes, including inhibitor and water. The model of (1) was generated from the crystal structure of TMQ and optimized with *SYBYL* (Tripos Inc., 1997). Between least-squares minimizations, the structures were manually adjusted to fit difference electron density and were verified by a series of omit maps calculated from the current model with deleted fragments. The final refinement statistics are summarized in Table 3. The Ramachandran conformational parameters from the last cycle of refinement generated by *PROCHECK* (Laskowski *et al.*, 1993)

Table 3
Crystal properties and refinement statistics.

	R3-1	R3-2	$P4_32_12$
Complex	Ternary	Binary	Binary
Unit-cell parameters			
a, b (Å)	85.87	85.43	62.93
c (Å)	77.51	78.36	95.74
Unit-cell volume (Å^3)	571564	571885	379144
V_M (Å^3 Da^{-1})	2.58	2.58	2.22
Solvent content (%)	52	52	45
Space group	$R3$	$R3$	$P4_32_12$
Resolution range (Å)	50.0–2.0	50.0–2.2	50.0–2.1
R_{merge} (%)	5.5	5.5	6.8
Completeness (highest resolution shell)	67.4	62.9	51.9
Overall completeness (%)	82.6	90.8	80.5
$F^2/\sigma(F)$	3.4	3.2	3.1
No. of reflections used to $2\sigma(I)$	9056	8857	8535
Total No. reflections observed	10192	10667	9522
R factor (%)	17.3	17.9	23.9
No. of protein atoms	1502	1502	1502
No. of water molecules	67	68	32
Ramachandran, % of residues in most favorable conformation	89.3	93.7	84.3
B factor (protein average) (Å^2)	25.67	23.87	28.59

Refinement statistics.

	R.m.s. σ.			
	R3-1	R3-2	$P4_32_12$	Target σ
Distances (Å)				
Bonds	0.018	0.019	0.025	0.020
Angles	0.055	0.053	0.070	0.040
Planar 1–4	0.054	0.058	0.072	0.050
Planar groups	0.014	0.014	0.017	0.020
Chiral volume	0.182	0.195	0.264	0.150
Single torsion	0.209	0.210	0.245	0.500
Multiple torsion	0.280	0.264	0.315	0.500
Possible hydrogen bonds	0.232	0.339	0.276	0.500
Torsion angles (°)				
Planar	2.4	2.6	3.0	3.0
Staggered	21.4	21.5	26.6	15.0
Orthonormal	21.6	22.1	26.9	20.0

Table 4
Inhibitor intermolecular contacts (Å) in hDHFR complexes.

Contacts (Å)	$R3$ hDHFR–NADPH–(1)	$R3$-1 hDHFR–(1)	$P4_32_12$ hDHFR–(1)	F31A hDHFR–TMQ†	hDHFR–NADPH–MTXT ‡
4NH2···Ile7 O	3.0	3.1	3.0	2.3	2.5
4NH2···Tyr121 OH	3.6	3.5	3.9	3.8	3.3
4NH2···Val115 O	3.1	3.1	3.2	4.0	3.0
2NH2···Thr136 O$^\gamma$	3.7	3.8	4.0	3.2	3.2
2NH2···water	3.7	3.7	—	—	3.2
2NH2···Glu30 OE2	2.8	2.8	2.5	3.0	2.9
N1···Glu30 OE1	2.9	2.9	2.9	3.2	2.6
Glu30 OE1···water	2.8	2.7	2.9	—	2.4
Glu30 OE2···Thr136 O$^\gamma$	2.7	2.7	2.8	3.2	3.2
Thr136 O$^\gamma$···water	2.8	2.9	3.4	2.8	—
Arg70 NH2···Gln35 NE2	2.9	2.9	3.4	4.0	—
Arg70 NH2···Lys68 O	2.9	2.8	3.1	3.2	2.6
Arg70 NH1···Thr38 O$^\gamma$	2.8	2.8	3.0	2.6	3.5
Trp24 NE1···water	3.1	3.4	3.3	—	3.2
N8···water	3.6	3.2	3.3	—	2.8
N8···Glu30 OE1	3.9	3.7	3.8	3.7	2.8

† Cody *et al.* (1993). ‡ Cody *et al.* (1992).

show that between 84 and 93% of the residues have the most favored conformation and none are in disallowed regions for these hDHFR complexes with (1).

3. Results

3.1. Overall structure

The overall folding characteristics of these hDHFR complexes with antifolate (1) are similar to those reported previously (Cody *et al.*, 1992, 1997, 2003; Gangjee *et al.*, 1998). When these structures were compared by a pairwise least-squares fit of the 35 active-site residues generated by *PROFIT* (Smith, personal communication), the major conformational changes between these different crystal forms involve movement (1.9–3.2 Å) of loop regions 44 (residues 40–48), 84 (residues 81–89) and 103 (residues 99–108) (Fig. 3). Similar but smaller differences in loop conformations have been described that result from ligand-induced changes on cofactor binding in ternary complexes of *Escherichia coli* DHFR (Sawaya & Kraut, 1997) and *pc*DHFR (Cody *et al.*, 1999, 2000). In these previous examples, the largest changes are in the flap region at loop 20–23, which opens and closes on cofactor binding. There is no evidence of such loop movement in these hDHFR structures.

3.2. Inhibitor binding

The interactions of the pyrido[2,3-*d*]pyrimidine ring of (1) preserve the overall pattern of interactions with invariant residues in the DHFR active site (Table 4; Fig. 4). As observed in other DHFR complexes with tight binding ligands, including that of TMQ (Cody *et al.*, 1992, 1993, 1997, 2003; Chunduru *et al.*, 1994; Lewis *et al.*, 1995; Oefner *et al.*, 1988; Davies *et al.*, 1990; Klon *et al.*, 2002), a hydrogen-bonding network that involves structural water, the conserved residues Trp24, Glu30, Thr136 and the N1 nitrogen, the 2-amine group and N8 nitrogen of inhibitor (1) is maintained, with the exception of the tetragonal structure, in which no structural water was observed with contacts to the inhibitor 2-amino group. Similarly, the inhibitor 4-amino group makes hydrogen-bonding contacts with the conserved residue Ile7 and weaker contacts to Tyr121 (Table 4). This network of hydrogen-bonding interactions involving the diaminopteridine or diaminopyridopyrimidine ring is characteristic of all crystal structures reported for DHFR complexes (Cody *et al.*, 1999; Sawaya & Kraut, 1997). Additional conserved contacts involve Arg70. As shown (Table 4), the amine groups of Arg70 form a network of contacts with the back-

bone of Lys68, the hydroxyl group of Thr38 and the functional group of Gln35.

Comparison of these hDHFR complexes reveals that the conformation of inhibitor (1) is nearly the same in all complexes, as well as being similar to that in the parent quinazoline TMQ (Fig. 4) (Cody *et al.*, 1993). Analysis of the interactions of the methoxy substituents of the benzyl ring of (1) shows that the 3′-methoxy group of (1) makes few close hydrophobic contacts. Most contacts are >4.0 A from residues Leu22, Pro26, Ile60 and Pro61. On the other hand, the 5′-methoxy group is involved in many more contacts with the active-site residues, in particular with Leu22, Phe34 and Leu67. Depending on the side-chain conformation of Gln35, the functional group makes close hydrophilic contacts with the 5′-methoxy O atom of the inhibitor. In general, there are also favorable hydrophobic contacts between the phenyl ring of Phe31 and the methoxybenzyl ring of the inhibitor.

The closest contacts of the 4′-methoxy group of (1) are made with Asn64 (4′-O$\cdots$N, 3.0 Å) (Fig. 4). These contacts are weaker in the tetragonal hDHFR structure than in the rhombohedral structures. The methyl of the 4′-methoxy group also makes favorable hydrophobic contacts with Phe31 and Pro61. In the *pc*DHFR and *tg*DHFR enzymes Asn64 is replaced by Phe and thus these enzymes should have more favorable interactions since the 4′-methoxy methyl could also make hydrophobic contacts with Phe69.

It is not clear what factors contribute most to the crystallization of a binary or ternary complex despite the incubation of the enzyme with the cofactor NADPH prior to crystallization. Analysis of the active-site interactions between the

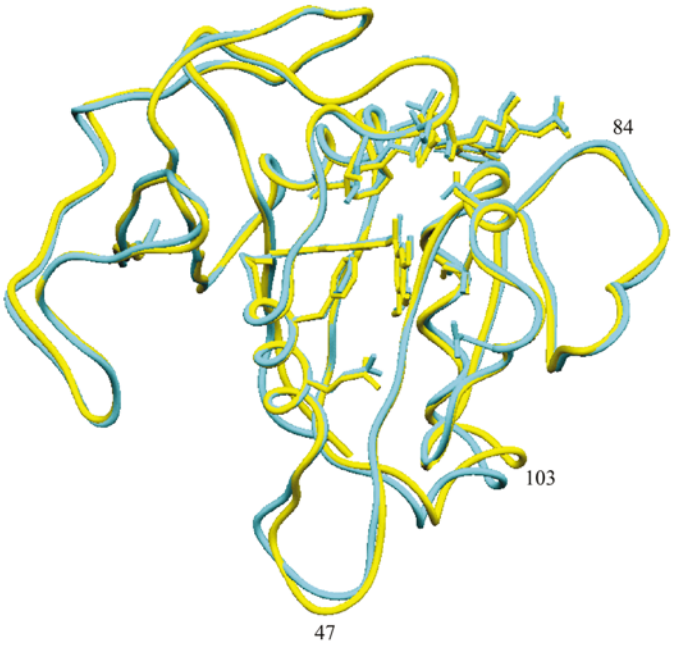

Figure 3
Superposition of the backbone atoms of hDHFR–NADPH–(1) (cyan) and the $P4_32_12$ hDHFR–(1) (yellow) complexes. Noted on the diagram are the loops that have the largest conformational differences between the two lattices. Models were produced with *SETOR* (Evans, 1993).

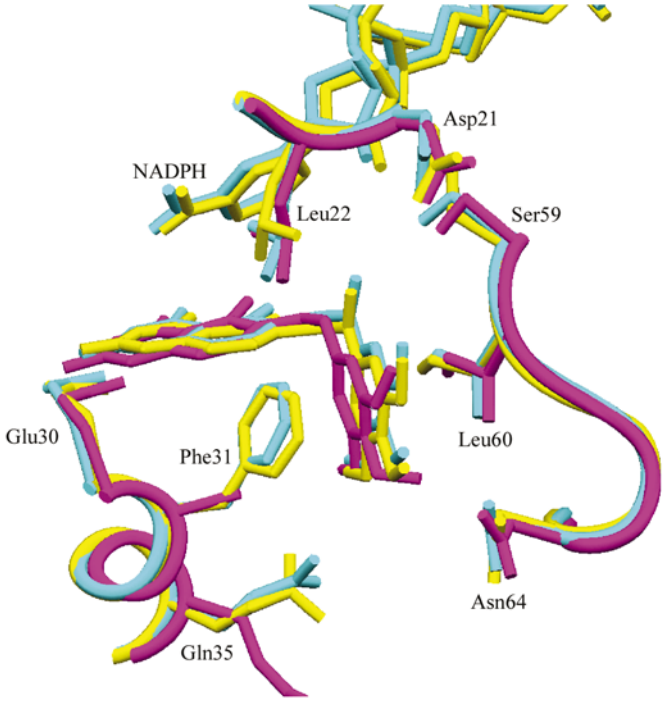

Figure 4
Comparison of active-site binding region of hDHFR with NADPH and antifolate (1) for the *R*3 lattice (cyan) and for the $P4_32_12$ lattice (yellow). Also shown is F31A hDHFR–TMQ (violet). Models were produced with *SETOR* (Evans, 1993).

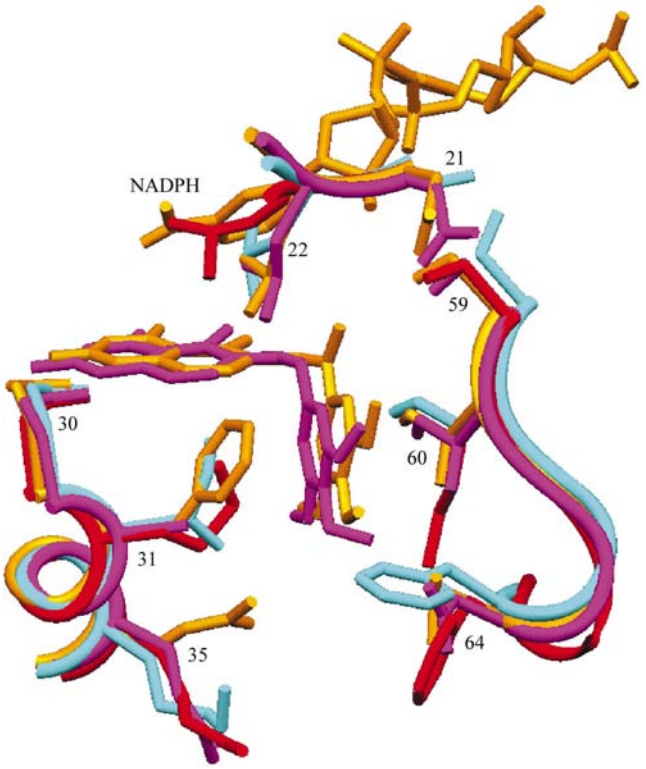

Figure 5
Comparison of the active-site region of hDHFR NADPH–(1) (gold), hDHFR F31A TMQ (violet) and pcDHFR (cyan) with a model of tgDHFR (red) highlighting residue changes at positions 21, 30, 31, 35, 60 and 64 (human DHFR numbering). Models were produced with *SETOR* (Evans, 1993).

binary complexes and the ternary complex shows that the contact distance between the nicotinamide C2 atom and the C5 methyl of inhibitor 1 is 3.3 Å for the ternary *R*3 lattice, whereas this distance is 3.0 Å when inhibitor (1) from the binary complex is modeled into the ternary complex and 2.8 Å for a model with TMQ.

3.3. Crystal packing

The observation of two different lattices for complexes of hDHFR with compound (1) provides an opportunity to compare the influence of packing interactions on the conformations of surface loops in these structures (Fig. 3). One monitor of changes in packing environment for the enzyme is the difference in the contacts of residue Lys63. In the *R*3 lattice, this residue is situated about the threefold symmetry axis and makes contacts of 7.6 Å to the NZ atoms of the side chains of the symmetry-related molecules in the ternary rhombohedral hDHFR complex. This value is 8.6 Å for the binary complex with (1) and 7.8 Å for the TMQ binary complex (Cody *et al.*, 1993). Changes in the side-chain conformation can have a significant effect on this contact, as shown in the structure of a binary complex of hDHFR with a N9—C10 reversed-bridge antifolate, in which this contact distance is only 4.3 Å (Cody *et al.*, 2003). This contact is 8.5 Å for the *R*3 lattice of the hDHFR–NADPH–MTXT ternary complex (Cody *et al.*, 1992), indicating that this structure is more loosely packed. In the tetrahedral lattice, this residue makes a twofold symmetry contact of 8.1 Å.

4. Discussion

This is the first observation of a hDHFR complex with a pyrido[2,3-*d*]pyrimidine analog (1) that has a similar conformation to that of the parent quinazoline, TMQ (Fig. 1). Analysis of the intermolecular packing contacts for these structures reveals that the tetragonal lattice is more tightly packed than the rhombohedral lattice and that the closer contacts give rise to differences in surface-loop conformations (Fig. 3). The largest conformational changes between these lattices are for loops 47 (2.2 Å), 84 (1.9 Å) and 103 (3.2 Å). These differences are greater than observed between two isomorphous *R*3 structures reported previously (Cody *et al.*, 2003).

Modeling studies of the interactions of the N10-substituted analogs (—H, —CH_3 and —CHO) indicate that the N10—CH_3 of (1) makes favorable hydrophobic contacts with the conserved residue Leu22 of hDHFR, whereas the N—CHO analog places the keto O atom in an unfavorable contact (2.6 Å) with this hydrophobic residue. On the other hand, the N—CHO analog can be orientated such that the keto O atom can make favorable hydrogen-bonding contacts with the ribose hydroxyl of NADPH or through a water-mediated contact to the conserved Ser59. In the case of the N10—H analog there are no close contacts, but a structural water could bind and form a hydrogen-bonding network with the ribose hydroxyl of NADPH, as well as to the conserved Ser59 hydroxyl, as was observed in the crystal structure of hDHFR with folate (Oefner *et al.*, 1988). In the case of *pc*DHFR, differences in the conformation of the loop containing Leu25 results in even more unfavorable contacts (1.7 Å). The potential contacts of the keto O atom with the ribose hydroxyl of NADPH are weaker because the nicotinamide-ribose ring is observed in a different conformation in many of the *pc*DHFR crystal structures (Cody *et al.*, 1997, 1999). Similar contacts are expected for the structure of *tg*DHFR, as there are few sequence changes in this region of the active site.

The preferential *tg*DHFR inhibitory potency for the trimethoxybenzyl ring-substitution pattern of this series is likely to be reflected in the favorable interactions of the 4′-methoxy group with the hydrophobic residues at positions 31 (Phe, Ile and Phe in hDHFR, *pc*DHFR and *tg*DHFR, respectively) and 60 (Ile, Ile and Met, respectively) (Fig. 5). In the case of *tg*DHFR, there is a greater potential for favorable interactions of the 4′-OCH_3 of (1) and the SCH_3 of Met87, which are not present in the other species. Differences in the electrostatic nature of the chlorobenzyl-substituted analogs are likely to play a role in the lower potency and selectivity of these analogs. Therefore, the methoxybenzyl ring-substitution pattern that interacts with the most highly variable sequences among these DHFR enzymes will have the greatest potential to impact on potency and selectivity. This is reflected in activity differences for inhibitor (1) in which the 3′-methoxy group interacts with variable environments at positions 21 and 31, in which the 4′-methoxy interacts with variable residues at positions 60 and 64 and in which the 5′-methoxy group encounters variable environments at position 35. The greater potency of these antifolates for *tg*DHFR may be the result of the greater conformational space in the *tg*DHFR structures that could result from the shift of loop 20, which enlarges the active site as shown for the *pc*DHFR structures (Cody *et al.*, 1999, 2000). The *tg*DHFR structure will presumably have more space in this region of the active site as there is a Gly substitution for the Asp of hDHFR and Ser of *pc*DHFR.

This work was supported in part by the National Institutes of Health grants GM-51670 (VC), AI41743 (AG) and AI44661 (AG).

References

Chunduru, S. K., Cody, V., Luft, J. R., Pangborn, W., Appleman, J. R. & Blakley, R. L. (1994). *J. Biol. Chem.* **269**, 9547–9555.
Cody, V., Chan, D., Galitsky, N., Rak, D., Luft, J. R., Pangborn, W., Queener, S. F., Laughton, C. A. & Stevens, M. F. G. (2000). *Biochemistry*, **39**, 3556–3564.
Cody, V., Galitsky, N., Luft, J. R., Pangborn, W. & Gangjee, A. (2003). *Acta Cryst.* D**59**, 654–661.
Cody, V., Galitsky, N., Luft, J. R., Pangborn, W., Gangjee, A., Devraj, R., Queener, S. F. & Blakley, R. L. (1997). *Acta Cryst.* D**53**, 638–649.
Cody, V., Galitsky, N., Luft, J. R., Pangborn, W., Queener, S. F. & Gangjee, A. (2002). *Acta Cryst.* D**58**, 1393–1399.
Cody, V., Galitsky, N., Rak, D., Luft, J. R., Pangborn, W. & Queener, S. F. (1999). *Biochemistry*, **38**, 4303–4312.

Cody, V., Luft, J. R., Ciszak, E., Kalman, T. I. & Freisheim, J. H. (1992). *Anticancer Drug Des.* **7**, 483–491.
Cody, V., Wojtczak, A., Kalman, T. I., Freisheim, J. H. & Blakley, R. L. (1993). *Adv. Exp. Biol. Med.* **338**, 481–486.
Davies, J. F., Delcamp, T. J., Prendergast, N. J., Ashford, V. A., Freisheim, J. H. & Kraut, J. (1990). *Biochemistry*, **29**, 9467–9479.
Evans, S. V. (1993). *J. Mol. Graph.* **11**, 134–138.
Finzel, B. C. (1987). *J. Appl. Cryst.* **20**, 53–55.
Gangjee, A., Shi, J., Queener, S. F., Barrows, L. R. & Kisliuk, R. L. (1993). *J. Med. Chem.* **36**, 3427–3443.
Gangjee, A., Vasudevan, A., Queener, S. F. & Kisliuk, R. L. (1996). *J. Med. Chem.* **39**, 1438–1446.
Gangjee, A., Vidwans, A. P., Vasudevan, A., Queener, S. F., Kisliuk, R. L., Cody, V., Li, R., Galitsky, N., Luft, J. R. & Pangborn, W. (1998). *J. Med. Chem.* **41**, 3426–3434.
Hendrickson, W. A. & Konnert, J. H. (1980). *Computing in Crystallography*, edited by R. Diamond, S. Ramaseshan & K. Venkatesen, pp. 13.01–13.25. Bangalore: Indian Academy of Sciences:.
Klon, A. E., Heroux, A., Ross, L. J., Pathak, V., Johnson, C. A., Piper, J. R. & Borhani, D. W. (2002). *J. Mol. Biol.* **320**, 677–693.
Laskowski, R. A., MacArthur, M. W., Moss, D. S. & Thornton, J. M. (1993). *J. Appl. Cryst.* **26**, 283–291.
Lewis, W. S., Cody, V., Galitsky, N., Luft, J. R., Pangborn, W., Chunduru, S. K., Spencer, H. T., Applemann, J. R. & Blakley, R. L. (1995). *J. Biol. Chem.* **270**, 5057–5064.
Masur, H., Polis, M. A., Tuazon, C. V., Ogota, A.D., Kovacs, J. A., Kaz, D., Hilt, D., Simons, F., Feuerstein, I., Lingren, B., Lane, H. C., Chabner, B. A. & Allegra, C. J. (1993). *J. Infect. Dis.* **167**, 1422–1426.
Mills, J. & Masur, H. (1991). *Sci. Am.* 50–57.
Oefner, C., D'Arcy, A. & Winkler, F. K. (1988). *Eur. J. Biochem.* **174**, 377–385.
Otwinowski, Z. & Minor, W. (1997). *Methods Enzymol.* **276**, 307–326.
Piper, J. R., Johnson, C. A., Krauth, C. A., Carter, R. L., Hosmer, C. A., Queener, S. F., Borotz, S. E. & Pfefferkorn, E. R. (1996). *J. Med. Chem.* **39**, 1271–1280.
Queener, S. F. (1995). *J. Med. Chem.* **38**, 4739–4759.
Roos, D. S. (1993). *J. Biol. Chem.* **268**, 6269–6280.
Sack, J. S. (1988), *J. Mol. Graph.* **6**, 244–245.
Sawaya, M. R. & Kraut, J. (1997). *Biochemistry*, **36**, 586–603.
Tripos Inc. (1997). *SYBYL* version 6.0. Tripos Inc., St Louis, MO, USA.
Wang, Y., Bruenn, J. A., Queener, S. F. & Cody, V. (2001). *Antimicrob. Agents Chemother.* **45**, 2517–2523.